Interface analysis and intrinsic thermal stability of MoO_x based hole-selective contacts for silicon heterojunction solar cells

Jinyoun Cho[a,b]*, Neerja Nawal[b], Afshin Hadipour[b], Maria Recaman Payo[b], Arvid van der Heide[b], Hariharsudan Sivaramakrishnan Radhakrishnan[b], Maarten Debucquoy[b], Ivan Gordon[b], Jozef Szlufcik[b] and Jef Poortmans[a,b,c]

[a]ESAT department, K.U. Leuven, Leuven 3001, Belgium

[b]imec (partner in EnergyVille), Kapeldreef 75, Leuven 3001, Belgium

[c] University Hasselt, Martelarenlaan 42, Hasselt 3500, Belgium

*Corresponding author: Jinyoun.cho@imec.be

Keywords: MoO_x, hole-selective contact, metal oxides, module, damp heat, interfacial dipole

Highlights

- MoO_x is used to replace p-a-Si:H at the hole contactin silicon heterojunction (SHJ) solar cells, leading to a reduction of parasitic absorption and a J_{SC} improvement on average of 0.5 mA/cm^2.
- Influence of MoO_x thickness and annealing condition on the SHJ cell performance was studied and optimal parameters were determined.
- Impact of MoO_x thickness and anneal treatment on the thin film interfaces at the hole contact was investigated and an interfacial dipole in the form of a-SiO_x was postulated.
- A glass to glass 1-cell mini-module was fabricated using a MoO_x-contacted SHJ cell.
- After damp-heat testing, good long-term stability was achieved at module-level, with a degradation of less than 3%$_{abs}$ (passing the IEC61215 standard).

Abstract

A possible research path to increase the photo-generated current in silicon heterojunction (SHJ) solar cells is to replace doped layers on the front-side of the cell, which result in significant parasitic light absorption losses. MoO_x is one candidate to replace the p-doped a-Si:H layer in such devices, although it is claimed to be relatively unstable to thermal treatments. We found that a MoO_x film with a thickness of 6 nm is sufficient to achieve a J_{SC} of 36 mA/cm^2, which is 0.5 mA/cm^2 on average higher than that of our classical SHJ reference cell. We also established a contact sintering condition for printed Ag at 160 °C after MoO_x deposition, without degrading the cell performance. The champion MoO_x-contacted cell yielded V_{OC} of 724 mV and FF of 74.1%, resulting in an efficiency of 19.3%. From a detailed analysis of the interfaces of the hole contact, an interfacial a-SiO_x of 1.6-2 nm was observed between a-Si:H and MoO_x irrespective of the MoO_x thickness (6 - 10 nm) before and after contact sinter annealing at 160 °C. We postulate that this a-SiO_x layer acts as an interfacial dipole layer and also increases the contact resistivity at this contact. The intrinsic stability of the optimised MoO_x-contacted cell is studied using a one-cell mini-module under standard damp-heat testing (85˚C/85% humidity/1000 h). More than 97 $\%_{rel}$ of the original efficiency is maintained after 1010 hours of testing, which is comparable to the behavior observed in a classical SHJ reference one-cell mini-module that was similarly tested.

1. Introduction

Two-side contacted silicon heterojunction (SHJ) solar cells are very attractive because of their high-efficiency potential combined with a relatively simple fabrication process [1]. Intrinsic hydrogenated amorphous silicon (i-a-Si:H) layers in SHJ solar cells provide excellent chemical surface passivation, while n-type or p-type hydrogenated amorphous silicon (n-a-Si:H or p-a-Si:H) layers induce band bending at the surface region of the c-Si substrate, which results in field-effect passivation. However, there are significant optoelectrical losses associated with a-Si:H, in particular when it is doped [2]. Due to its quasi-direct band structure, a-Si:H has a high absorption coefficient [3]. Since only a small part of the photo-generated minority carriers in the a-Si:H layers of SHJ cells will get collected and contribute to the photogenerated current, a substantial optoelectrical loss cannot be avoided [2,4].As an alternative heterojunction structure, metal-oxide-based passivating contacts have recently received quite some attention because their high band gap, typically above 3 eV [5], possibly reduces the parasitic absorption typically observed for a-Si:H based contacts in SHJ solar cells. Thus, by applying appropriate metal oxides, the use of doped layers for inducing band bending in SHJ solar cell can be avoided [5–12], and accordingly, the total parasitic absorption in a-Si:H can be reduced. Especially, as a hole-selective contact, MoO_x has been studied intensively because the high work function of MoO_x induces an upward band bending at the c-Si surface for hole collection [13–19], and has resulted in high cell efficiencies above 22 % [20]. However, MoO_x is known to exhibit weak stability in the presence of air, moisture and thermal treatment, leading to a degradation of hole selectivity and decrease in fill factor (FF) and open circuit voltage (V_{OC}) of the eventual solar cell [15,20,21]. Therefore, several research groups have studied the thermal stability of MoO_x-contacted SHJ cells. One of the proposed reasons for this degradation is the effusion of H from surrounding layers, particularly i-a-Si:H. Essig et al. have reported that a pre-annealing of i-a-Si:H before MoO_x deposition leads to improved thermal stability by reducing the hydrogen-related degradation of MoO_x, which results in weak band bending at the hole contact region due to the lowered work function of the MoO_x [22,23]. In addition, annealing in an Ar atmosphere has been shown to minimize the stoichiometric reduction of MoO_x, which also lowers the work function of MoO_x [24,25]. In another approach, stacking MoO_x with a high work function metal, e.g. Ni, has also enabled higher thermal stability while annealing up to 300 °C for 10 min [26]. Moreover, Bullock et al. have shown that by using pre-annealing before MoO_x deposition, more than 95% of the initial cell efficiency of MoO_x-contacted solar cells can be retained after damp heat testing for 1000 hours [6]. However, all these studies have been done at cell level with additional treatment or special techniques. Thus, studying the intrinsic stability of MoO_x in SHJ solar cell would be interesting, and is one of the aims of this work.

When solar cells with MoO_x contacts are encapsulated in a module, degradation of the MoO_x contact related to the moisture and oxygen would be significantly reduced thanks to the hermetic glass/EVA protection. On the other hand, one should consider that these solar cells will experience additional thermal stresses during module fabrication and during operation in the field, which could have a negative impact on the MoO_x contacts. Therefore, understanding the thermal stability of the MoO_x-based contacts at module level is very important and more relevant than at cell level, which forms the second main goal of this work.

In this paper, we investigate the impact on the cell results of different process conditions, such as 1) MoO_x thickness, and 2) thermal budget (annealing temperature and time). Based on this, we determine the lowest possible annealing temperature for sintering of the printed Ag contact. We then integrate the optimized MoO_x layers into SHJ cells and investigate the interface of the MoO_x contacts before and after annealing, and for different MoO_x thicknesses. We also fabricate a glass to glass module to study the intrinsic stability of MoO_x contacts at module level via the damp-heat testing method (85 ˚C, 85 % humidity, 1000 h). All results are compared with reference classical SHJ devices.

2. Experiment

2.1. Preparation of test samples and solar cells

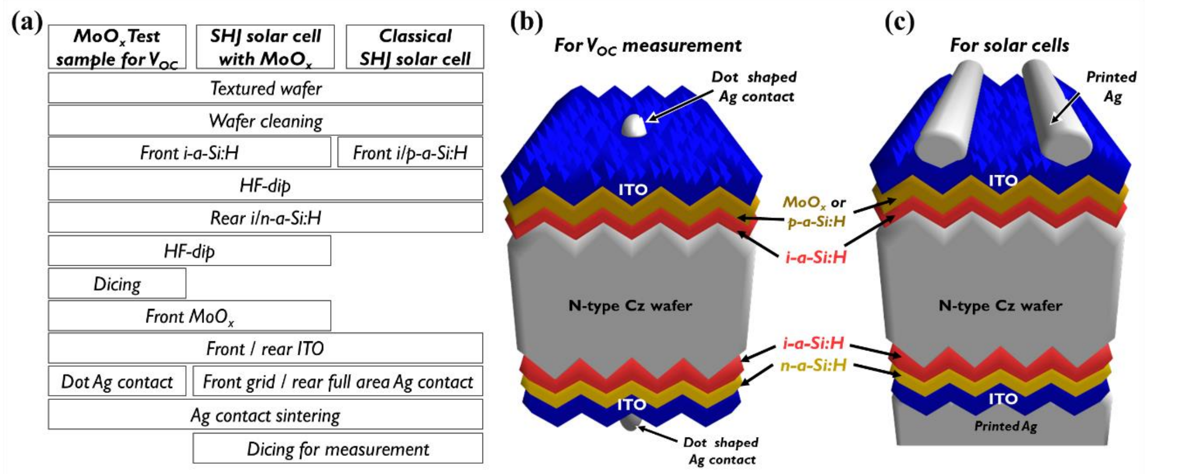

Figure 1. (a) Process flow for sample fabrication. Schematic sample structures for (a) V_{OC} test samples and (b) solar cells

As shown in Figure 1, test samples and solar cells were prepared using double-side textured (4.7 Ω·cm, 180 μm thickness) n-type Cz-Si wafers. After wafer cleaning using O_3/HCl/deionized water and HF/HCl solutions, 8 nm-thick intrinsic a-Si:H was deposited by plasma enhanced chemical vapor deposition (PECVD) on the front side of the all samples, while an additional 8nm thick p-a-Si:H was deposited on top of this i-a-Si:H for the classical SHJ samples only. After a short HF dip, an i/n-a-Si:H stack layer was deposited on the rear side of all samples. The MoO_x V_{OC} test wafers were diced into 50 x 50 mm^2

test samples for studying the effect of MoO_x thickness and post-annealing conditions on V_{OC}. After an HF dip, MoO_x layers with various thicknesses were thermally evaporated on the front side of the MoO_x test group, using a MoO_3 powder (99.5%, Sigma-Aldrich) after reaching a base vacuum pressure of 2×10^{-6} Torr. Then, ITO was sputtered on the front and the rear side of all test samples with metal masks. Small dot contacts were formed on both sides using a Ag paste. These V_{OC} test samples were annealed in N_2 atmosphere using a rapid thermal annealing (RTA) tool at various temperatures and for various times. The real substrate temperature during RTA was monitored by a thermocouple. The Suns-Voc technique was used to measure the V_{OC} of these test samples at 1 sun.

For the fabrication of solar cells shown in Figure 1 (a) and (c), most processes are identical with the fabrication process for the test samples. For the SHJ cells, the i-a-Si:H thickness on the front was 8 nm (unless otherwise specified). A front metal grid and a full-area rear Ag metallization were applied using screen-printing. Screen-printed Ag contacts were annealed in a belt furnace at various temperatures for the cells shown in Figure 4 or at 160 ˚C for the cells shown in Figure 5. The temperatures given in the paper for the belt furnace annealing treatment are the real temperatures and not the set temperatures. All reported cells have an active cell area of 4 × 4 cm^2. Illuminated IV curves were measured with an aperture opening of 4 × 4 cm^2 under calibrated illumination (AM 1.5G, 1000 W/m^2 at 25 °C). External quantum efficiency (EQE) and reflectance were measured using a spot size of 1.5 × 1.5 cm^2 for the wavelength from 280 nm to 1200 nm with the step of 10 nm. Therefore, the EQE and reflectance results include the shading and reflecting effects of the metal grid.

For TEM and EDX measurements, separate samples were prepared using a mirror-polished Cz wafer (~1 Ω·cm, 730 μm thickness). The same layer stack on the front was prepared following the same procedure shown in Figure 1 (a).

The interfacial layers, and their chemical component distribution were analyzed by using transmission electron microscopy (TEM), energy-dispersive X-ray spectroscopy (EDX).

2.2. Preparation of one-cell mini-module

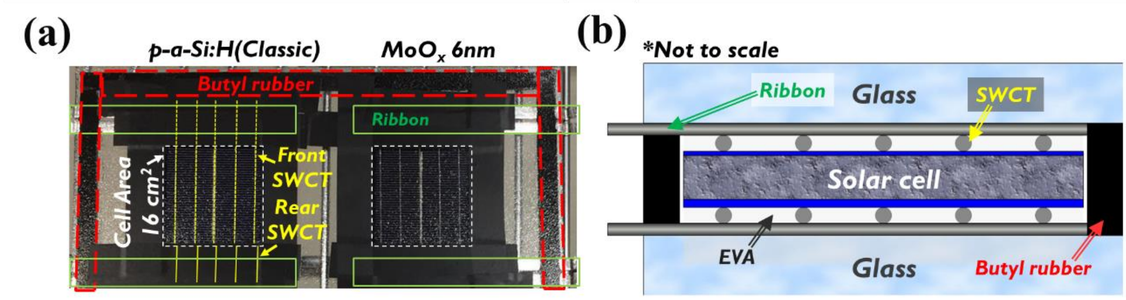

Figure 2. (a) Photograph of the as-fabricated one-cell mini-modules (cell size 4 cm x 4 cm) . (b) Schematic cross-section of the mini-module which includes a solar cell, cover glasses, ethylene vinyl acetate (EVA), smart-wire connection technology(SWCT), ribbon and butyl rubber.

One-cell mini-modules (glass to glass) were fabricated, one with a 6 nm-thick MoO_x contacted cell and the other with a classical SHJ cell for comparison (see Figure 2 (a)). An UV-blocking ethylene vinyl acetate (EVA) sheet, a smart-wire connection technology (SWCT) foil (Meyer Burger), ribbons and glass were used for encapsulation. A butyl rubber tape was was applied for hermetic edge sealing (see Figure 2 (b)). The lamination process was carried out at 150˚C for about 20 min. During the course of the damp heat testing (85˚C/85% humidity/1000hour), illuminated IV curves (AM 1.5, 1000 W/m^2 at 25 °C) were measured after every 250 hours. An aperture area of 4×4 cm^2 was used for these measurements by using an opaque black tape around the edge of the active cell area (see photograph in Figure 2 (a)).

3. Results

3.1. Determination of the optimal MoO_x thickness and the highest possible annealing temperature for MoO_x contact cells

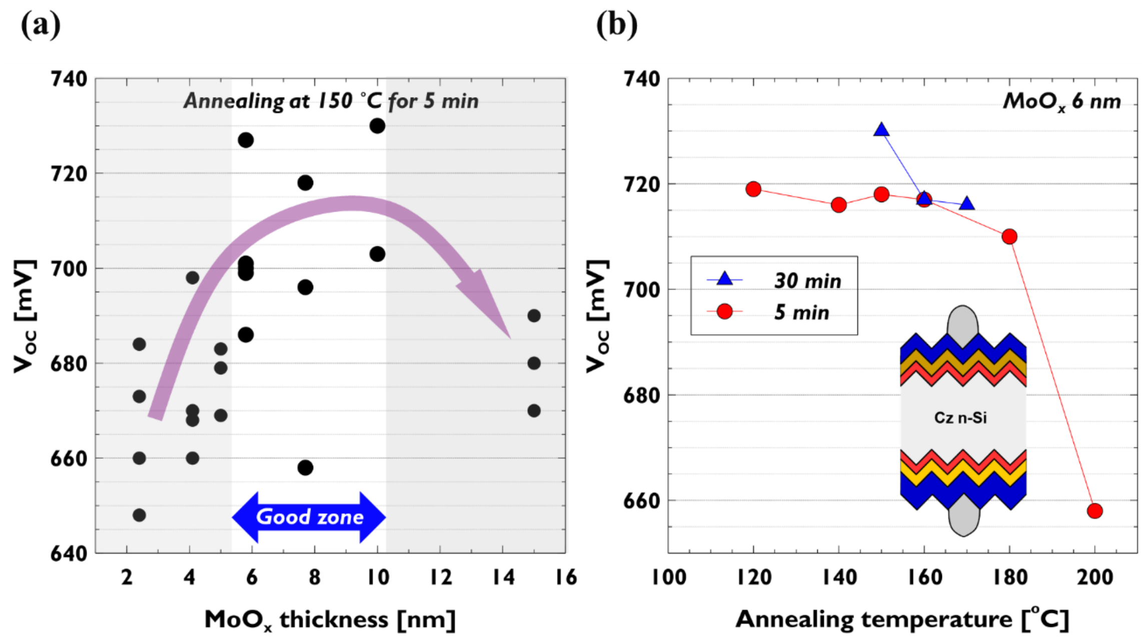

Figure 3. (a) V_{OC} comparison as a function of MoO_x thickness and (b) Voc dependence on the annealing temperature of the Ag sintering process.

The MoO_x thickness is as important as p-a-Si:H thickness in SHJ cells to achieve efficient hole collection [21]. A sufficiently-thick MoO_x layer is required to induce strong upward band bending while a thin layer is desired to achieve a low series resistance (R_s) in the cells due to the high intrinsic resistivity of the MoO_x layer of 10^8 - 10^{10} Ω·cm [27]. As can be seen in Figure 3 (a), the V_{OC} of the test samples varies as a function of the thickness of the MoO_x layer. Although data points are largely scattered, the optimum thickness of the MoO_x is found to be between 6 and 10 nm.

To serve as a hole contact, it is important that the MoO_x layer maintains its high work function to achieve high upward band bending at the contact region [16]. However, the high work function of the layer is easily reduced by oxygen movement from MoO_x to Si (or a-Si:H as in this study) during annealing [28]. To study the impact of the annealing condition, an RTA tool was used to achieve a well-controlled temperature profile instead of the belt furnace which typically shows some temperature fluctuations.

Finding an upper limit for the annealing temperature is important to avoid degradation of the MoO_x during further processing. According to the results shown in Figure 3 (b), an annealing temperature above 180˚C leads to a drastic drop in V_{OC}. Until 160 °C, a high V_{OC} above 716 mV is maintained. Even when annealing times up to 30 min were used, high V_{OC} values were obtained at a temperature between

150 and 170 °C. We can, therefore, conclude that it is better not to use process temperatures above 170 °C, which is in line with results reported elsewhere [20,21].

3.2. Determination of the minimum required annealing temperature for classical SHJ cells

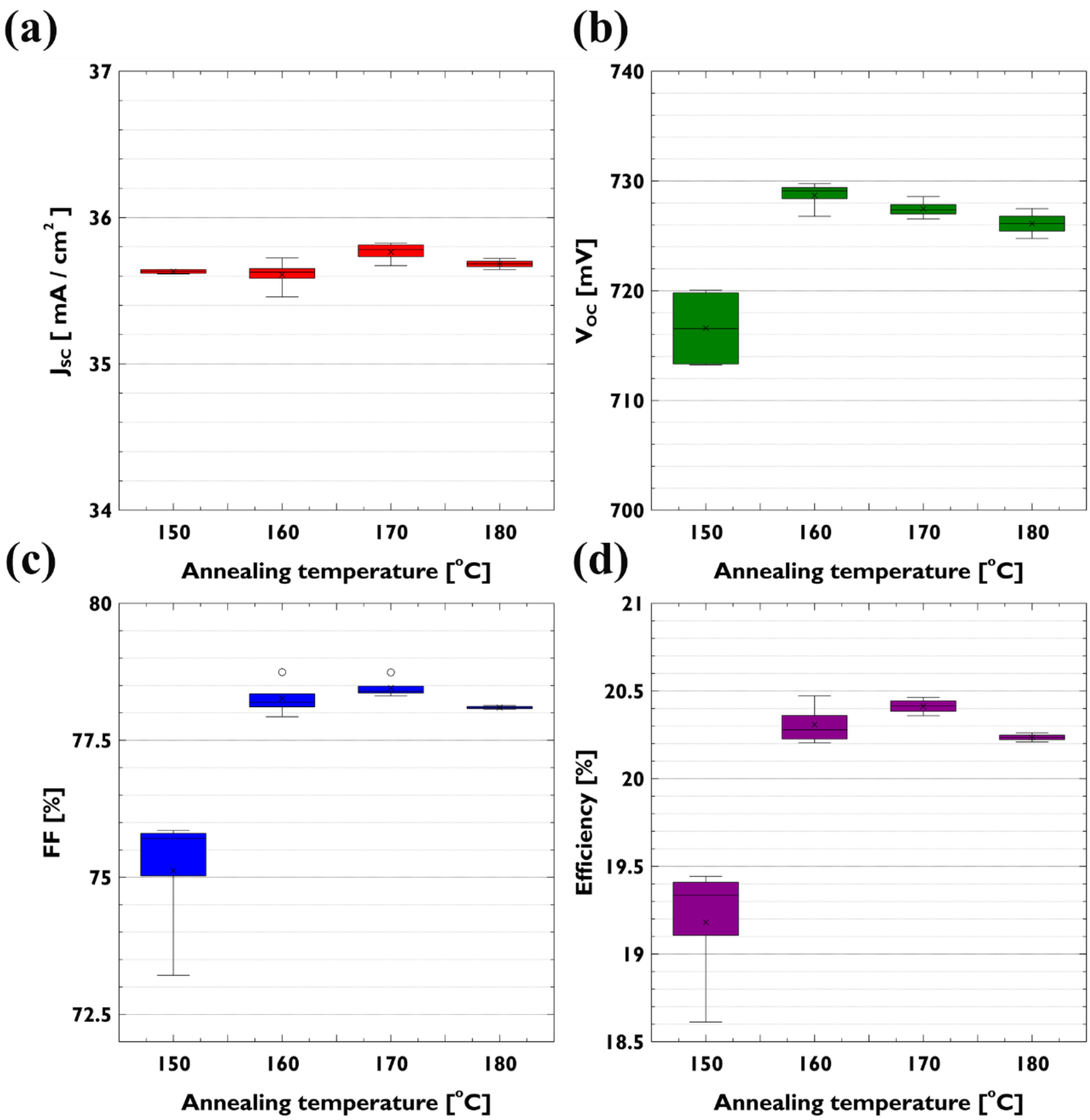

Figure 4. Illuminated IV parameters of the classical SHJ cells after annealing cells at different temperatures in a belt furnace. (a) Jsc, (b) Voc, (c) FF and (d) efficiency.

Although process temperatures below 170 °C could limit the degradation of the MoO_x layer in SHJ solar cells, a certain minimal thermal budget is required to 1) recover sputter damage during ITO deposition, 2) to achieve a low line resistance of the printed Ag contacts, 3) to make an ohmic contact between ITO and Ag, and 4) to improve ITO conductivity [29].

To investigate the minimum required annealing temperature, classical SHJ cells were prepared with thinner i-a-Si:H layers of 5 nm thickness on the front to induce more sputter damage to the samples [30], so that the impact of annealing condition on V_{OC} and other parameters would be seen more clearly. These cells were then annealed in a belt furnace at different temperatures from 150˚C to 180˚C. The annealing time in the hot zone is about 25 min. As shown in Figure 4, the cell performance is significantly poorer when the annealing temperature was below 160˚C. From 160˚C onwards, high V_{OC}, FF, and efficiencies could be obtained. Combining the results of Section 3.1 and 3.2, we can conclude that annealing temperatures in the range of 160-170˚C appear to be optimal in avoiding significant MoO_x degradation and simultaneously achieving good Ag-ITO contacts while also recovering ITO-related sputter damage. Annealing times up to 30 min have been tested. Since optimal process condition is relatively narrow, annealing temperature has to be carefully monitored.

3.3. MoO_x contact integration into SHJ solar cells

3.3.1 Comparison of cell results

In section 3.1, we identified the optimum thickness of the MoO_x layer in SHJ devices to be in the range of 6-10 nm. A thickness difference of a few nm can, however, lead to significant variations in device performance of such cells. Moreover, parasitic absorption of light in the MoO_x layer is still present due to the defect energy levels in the band gap [13,31]. Therefore, a thinner film is preferred for both electrical and optical reasons.

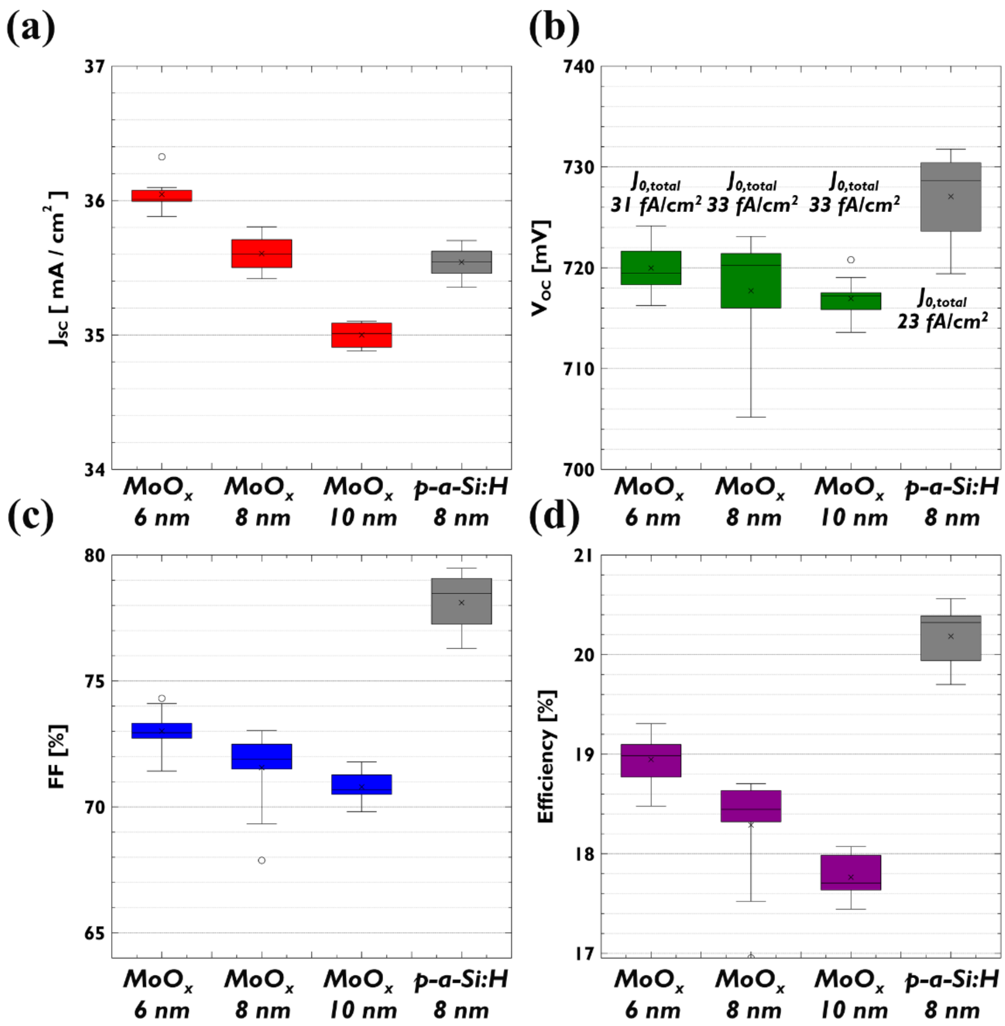

Figure 5. Illuminated IV parameters of MoO_x-contacted SHJ solar cells with different MoO_x thickness compared to classical SHJ cells with a p-a-Si:H layer. (a) J_{SC}, (b) V_{OC}, (c) FF and (d) efficiency.

In Figure 5, we compare the illuminated I-V results of MoO_x-contacted SHJ cells with different MoO_x thicknesses, and also a classical SHJ cell with p-a-Si:H. As shown in Figure 5 (a), the thinner the MoO_x film, the higher the resulting J_{SC}. This result clearly shows that some degree of parasitic absorption indeed occurs in the MoO_x film. The J_{SC} reduces as a function of MoO_x thickness by about 0.26 mA/cm^2 per nm, which is higher than the 0.13 mA/cm^2 per nm reported in the literature (for the case of cells annealed at 180°C) [21]. This means that the MoO_x layers we use in this study are more defective. Typically, defects in the MoO_x layer are generated by oxygen loss from the MoO_x layer [25] which may happen during thermal evaporation, or from H_2O effusion by the reaction of H from a-Si:H with O from

MoO_x [22,32]. Despite the observed parasitic absorption, SHJ cells with 6 nm thick MoO_x show J_{SC} of about 0.5 mA/cm^2 higher on average than the Jsc of the classical SHJ reference cells. A detailed loss analysis is given in Section 3.2.2.

Figure 5 (b) shows the V_{OC} and $J_{0,total}$ values of the classical SHJ cells and the MoO_x contact cells with different MoO_x thicknesses. The $J_{0,total}$ values were determined using the average J_{SC} and V_{OC} values of each group. A weak decreasing trend in V_{OC} is seen with increasing MoO_x thickness. However, considering the $J_{0,total}$ values of the three MoO_x groups are similar, the passivation quality of these cells should be similar. Thus, the decreasing trend in V_{OC} is attributed to the decreasing trend in J_{SC} with increasing MoO_x thickness. As shown in Figure 5 (c), thicker MoO_x layers also result in lower FF. A detailed FF loss analysis is given in Section 3.2.3.

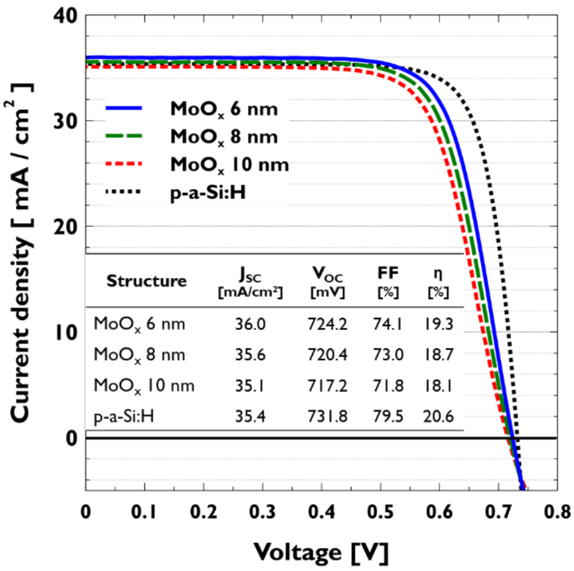

Figure 6. Champion solar cells with different MoO_x thickness in comparison to the best classical SHJ reference cell.

Illuminated IV curves of the champion cells of each split are shown in Figure 6. MoO_x-contacted SHJ cells show slightly S-shaped curves in contrast to the classical SHJ solar cells. Thinner MoO_x layers result in weaker S-shaped curves, and these cells, therefore, exhibit higher FF and V_{OC}. A detailed discussion about the development of an S-shaped light-IV curve and FF reduction is given in Section 3.2.4.

3.2.2 Optical losses: J_{sc} loss analysis

To understand the optical losses in the MoO_x-contacted solar cells, a detailed analysis was done following the method of Paviet-Salomon et al., which is based on EQE and reflectance data [33]. Since full area metallization was applied on the rear, the loss due to light transmittance through the rear side was assumed to be zero.

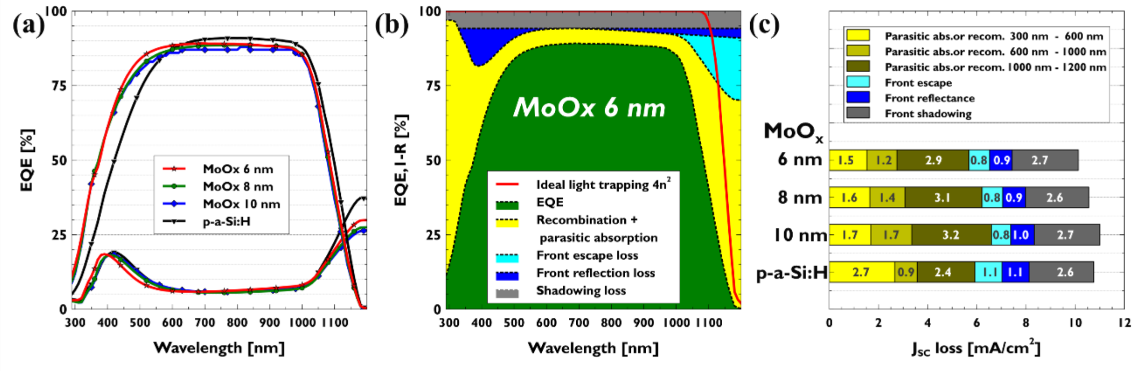

Figure 7. (a) EQE and reflectance of SHJ cell with different MoOx thickness and p-a-Si:H (measurement step size: 10 nm). (b) An example of the spectral J_{SC} loss analysis for a 6 nm-thick MoO_x-contacted SHJ cell. (c) Overview of J_{SC} loss factors for the different solar cells.

EQE and reflectance curves are compared in Figure 7 (a). The cells with MoO_x contact shows the gain in the EQE at short wavelength region (300 nm-600 nm) compared that of the classical SHJ cell with p-a-Si:H due to lower parasitic absorption. On the other hand, classical SHJ cell shows higher EQE than that of cells with MoOx at middle and long wavelength (600 nm-1200 nm). As an example, the J_{SC} loss analysis results of the cell with a MoO_x layer of 6 nm is shown in Figure 7 (b), and absolute loss values of the different cells are summarized in Figure 7 (c). The parasitic absorption within MoO_x is non-negligible, as observed with the reduction of EQE with thickness throughout the whole wavelength range of 400-1000 nm, and especially, at short wavelength range of 400-600 nm. A similar trend in absorption of MoO_x can be found in [34]. The sub-gap states of the MoO_x could be involved in this parasitic absorption. According to the literature [20,35], after annealing in an N_2 atmosphere, which is the case for this study, the absorbance of the MoO_x layers in the middle and long wavelength regions can be significantly increased due to the appearance of sub-gap states induced by loss ofoxygen in MoO_x. The reason for the lower front escape loss in MoO_x-contacted cells compared to the classical SHJ cell would also be due to MoO_x parasitic absorption.

3.2.3. Resistive losses: fill factor loss analysis

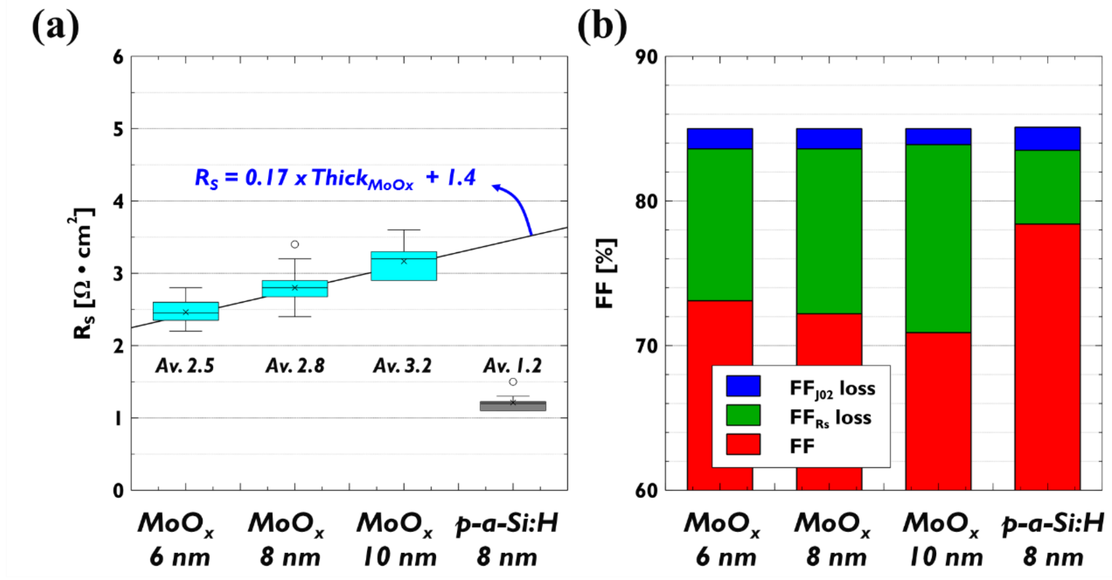

Figure 8. (a) Series resistance of solar cells with different thickness of MoO_x as hole contacts. (b) averaged fill factor losses of the cells in each group.

A FF loss analysis was carried using the method of Khanna et al. [36], based on the series resistance (R_S) as determined by the Bowden method [37], and the shunt resistance (R_{Shunt}) obtained by Suns-V_{OC} measurements. As shown in Figure 8 (a), R_S of the cells increases with increasing MoO_x thickness. Although the MoO_x layers contain defects which may help carrier conduction by trap-assisted tunneling through the layers [16], the MoO_x thickness is still a major factor determining the R_S of the cells. Each nm increase in thickness raises the total R_S of the cells by about 0.17 $\Omega{\cdot}cm^2$. The y-intercept of 1.4 $\Omega{\cdot}cm^2$ of the trend line in Figure 8 (a) indicates the R_S of the cells when no MoO_x would be present. However, this value of 1.4 $\Omega{\cdot}cm^2$ is still higher than the R_S of 1.2 $\Omega{\cdot}cm^2$ of the classical SHJ cell. The cause of the additional resistance could be related to interfacial a-SiO_x formation which will be discussed in Section 3.2.4.

In Figure 8 (b), the average fill factor losses of the cells in each group are shown. The FF_{Rshunt} loss is not shown in Figure 8 (b) because it was a very minor loss factor. The FF loss of the MoO_x contacted cells mainly came from the high R_S of the cells. The FF loss due to J_{02} is also comparable to those of the classical SHJ solar cells. The high R_S of the MoO_x-contacted cells is the main limitation affecting the final efficiency of these type of cells.

3.2.4. Interface analysis and charge transport in MoO_x hole contact

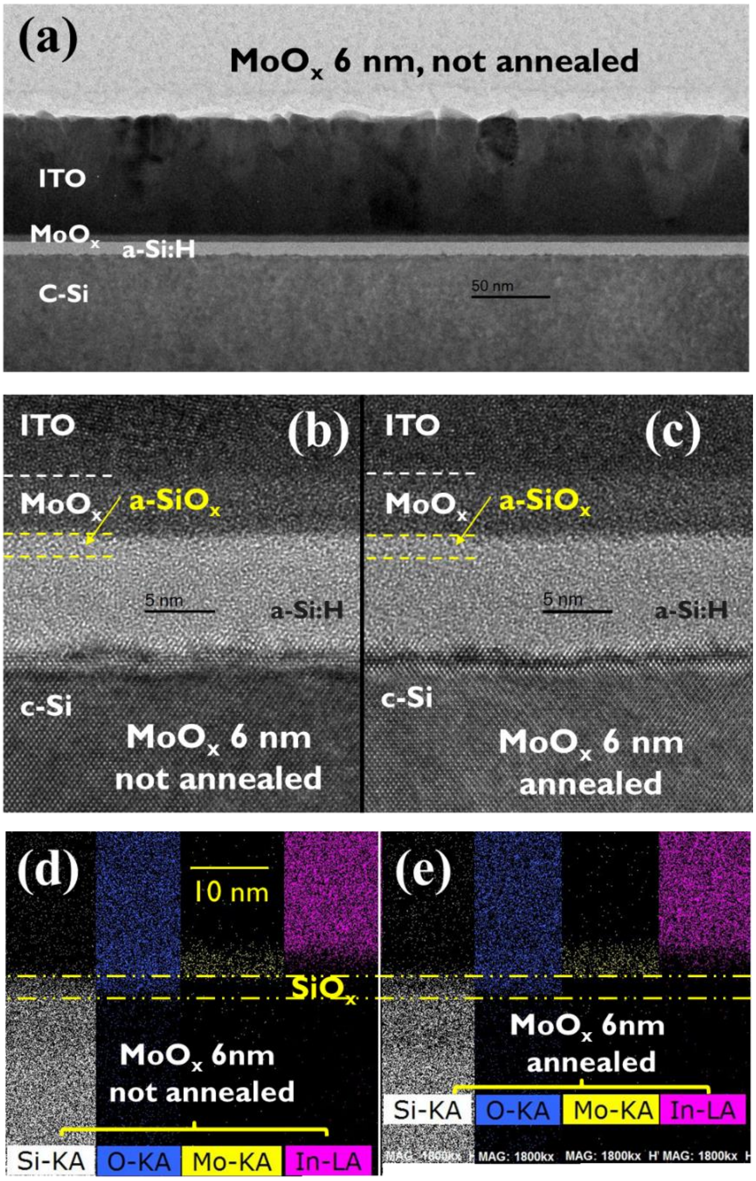

Figure 9. TEM analysis at the hole contact region of a 6 nm thick MoO_x contacted SHJ cell. (a) - (c) contact layers cross-section imaged by TEM, and (d) (e) chemical component distribution measured by EDX. (b), (d) correspond to the contact before annealing- and (c), (e) to after annealing, respectively.

The interface features of the MoO_x contact were investigated by TEM and EDX as a function of MoO_x thickness (6, 8, and 10 nm) in order to understand the underlying reasons for the reduction of FF and V_{OC}. Only the case of the hole contact with MoO_x thickness of 6 nm is shown in Figure 9. All other

TEM images and EDX measurement results have been appended as supporting information to this paper. For the contact with MoO_x thickness of 6 nm, the interfacial region was also compared before and after annealing.

Figure 9 (a) shows the contact layer structure consisting of i-a-Si:H, MoO_x and ITO. The TEM images of Figure 9 (b) and (c) shows the nano-scale features of the contact in high resolution, which reveals the presence of an a-SiO_x layer at the interface between MoO_x and i-a-Si:H. This is also confirmed by EDX measurements (Figure 9 (d) and (e)). The interfacial a-SiO_x formation is in agreement with reports on MoO_x/i-a-Si:H [13] or MoO_x /c-Si interfaces [38–40]. The thickness of the interfacial a-SiO_x was determined to be ~1.6 - 2 nm for all cases i.e. before/after annealing and different MoO_x thicknesses of 6, 8 and 10 nm. In other words, the interfacial a-SiO_x thickness is independent of the MoO_x thickness and is not increased by the thermal budget used for contact sintering.

Being an insulator, a-SiO_x poses a higher energy barrier for hole conduction compared to a-Si:H, due to its larger band gap [41,42]. This energy barrier at the hole contact is an important contributing factor that results in higher R_S and lower FF in the MoO_x-contacted cells compared to classical SHJ cells. However, this does not explain the increase in R_S and FF with MoO_x thickness, since the thickness of a-SiO_x is independent of MoO_x thickness. For this, we must consider the charge carrier transport through the entire hole contact structure. Hole collection in the cells with MoO_x contact is achieved by recombination, at the interfacial region between i-a-Si:H and MoO_x, of holes collected and transported through i-a-Si:H with electrons coming through the ITO and MoO_x layer, which are n-type materials. It is postulated that the main transport mechanism through MoO_x is trap-assisted tunneling, which decreases with increasing MoO_x thickness. As a result, it is expected that the R_S would increase as the MoO_x thickness is increased.

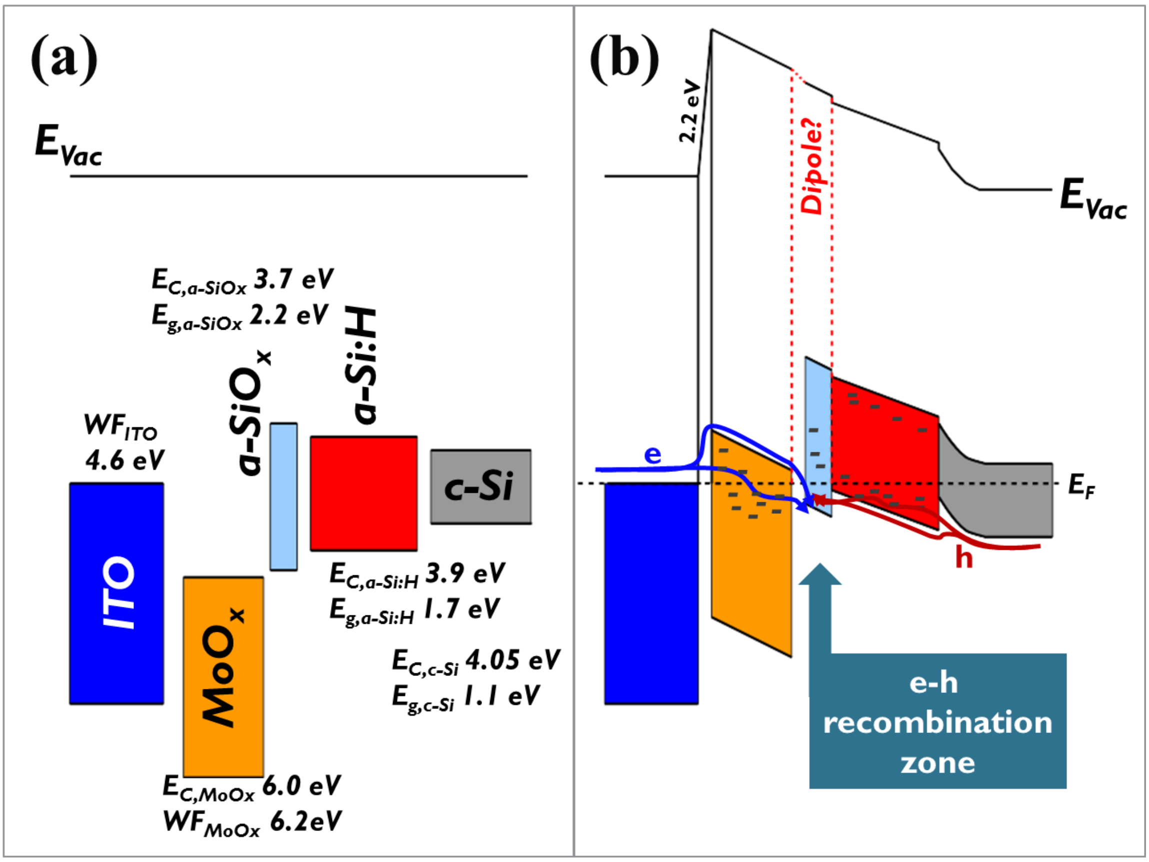

Figure 10. Material parameters and relative position are described in Figure (a). The a-SiOx energy band parameters are from the literature [42]*. (b) Proposed band diagram for MoOx based hole contacts based on the information in* [43].

Based on this discussion, a band diagram is proposed for MoO_x hole contact (Figure 10). The energy band structure at the hole contact is described in Figure 10 (a) and (b) before and after contact formation, respectively. Considering the strong dipole at MoO_x/ITO interface of about 2.2 eV [43], E_C of MoO_x could be positioned at a higher level than E_F of ITO. According to this band diagram (Figure 10 (b)), as MoO_x thickness increases, hole collection would be more inefficienct due to decreased probability of trap-assisted tunneling, and increased effect of the Schottky energy barrier between MoO_x and ITO [20]. This also leads to the S-shaped curve in the illuminated I-V characteristics (see Figure 6).

As for the c-Si substrate side, upward band bending would occur because of the high work function of MoO_x. To satisfy the continuity of the vacuum energy level between i-a-Si:H and MoO_x, another dipole seems to be required between MoO_x and i-a-Si:H. We propose that the a-SiO_x between i-a-Si:H and

MoO_x (Figure 9 (c))acts as a part of an interfacial dipole, which could reduce band bending at the c-Si surface and thus lead to slight loss in V_{OC} due to reduction in carrier selectivity [21,44].

To enhance the performance of MoO_x-based hole contact, firstly, the formation of the thick interfacial SiO_x sub-layer must be avoided to prevent detrimental R_S increase. This could be achieved by etching the native oxide before MoO_x deposition and by using the lowest possible annealing temperature after MoO_x deposition. Moreover, chemical termination of the a-Si:H surface may be used to achieve thinner a-SiO_x by reducing the reaction between Si in a-Si:H and oxygen in MoO_x [31,45]. In addition, Essig et al.[46] found that high base vacuum pressure during the thermal evaporation, and residual H_2O before MoO_x deposition have an impact on the FF. Secondly, the thickness of the MoO_x must be minimised to enhance the transport through this type of hole contact.

4. Intrinsic stability of MoO_x contacts at module level

To test the stability of MoO_x contact cell at module level, glass to glass one-cell mini-modules were fabricated using a cell with 6 nm thick MoO_x and a reference classical SHJ cell, respectively. Damp-heat test (85˚C, 85% humidity, 1000 hour) was carried out on these mini-modules.

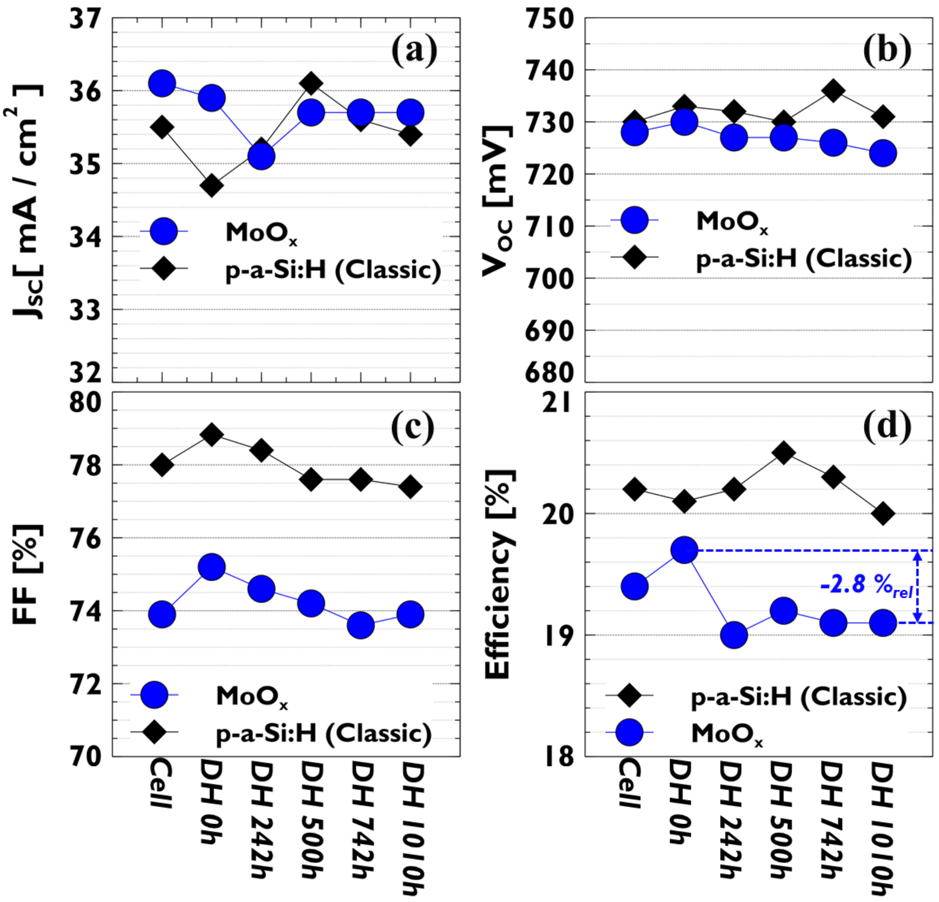

Figure 11. Illuminated IV parameters of MoOx-contacted and classical SHJ one-cell mini-modules under damp heat testing conditions, compared to the initial value at cell level before encapsulation. (a) J_{SC}, (b) V_{OC}, (c) FF and (d) efficiency.

As shown in Figure 11, the illuminated IV parameters of the mini-modules during damp heat testing were measured regularly over the course of 1010 hours. The MoO_x-contacted cell did not degrade after encapsulation as can be seen from the data point at DH 0h, which showed that the cell can withstand the thermal budget of module lamination. Although some fluctuations are observed in the results, the MoO_x-contacted device was very stable and showed a similar trend as compared to the classical SHJ device. After 1010 hours of damp heat testing, the MoO_x-contacted cell maintained 97.2 $\%_{rel}$ of its original efficiency at DH 0h. Therefore, it passes the reliability testing standard criteria of IEC 61215 which stipulates a power loss after 1000 hours of testing below 5 %. Other reliability tests at a module level, such as a thermal cycling tests, should be performed to enable us to judge whether a contact formation technology based on metal oxides can be viable.

5. Conclusions

MoO_x can serve as part of a hole-selective contact in SHJ solar cells because of its high work function and its transparent characteristics. However, care needs to be taken regarding the thermal budget that is used after MoO_x deposition because of the thermal instability of hole contacts incorporating MoO_x. Thermal stability of MoO_x-based hole contact has been proven in the temperature range of 160-170˚C up to 30 min, without any pre-deposition anneal. Therefore, an optimum annealing condition of 160˚C for 25 min was used for printed Ag sintering, which is sufficiently high for making a good Ag contact and sufficiently low for avoiding degradation of MoO_x. Integration of a 6 nm-thick MoO_x layer at the front of SHJ solar cells led to an improved J_{SC} compared to a classical SHJ cell of ~0.5 mA/cm^2 on average, due to lower parasitic absorption in MoO_x contact cells. The best MoO_x-based cell achieved a V_{OC} of 724 mV, a FF of 74.1 % and an efficiency of 19.3%. When the interface between MoO_x and i-a-Si:H was examined, an interfacial a-SiO_x was found with a thickness of 1.6-2 nm for all cells, irrespective of the MoO_x thickness and additional thermal treatment. This a-SiO_x layer is suspected of acting as a dipole layer which reduces upward band bending which is related to low V_{OC}. A one-cell mini-module was prepared to investigate the intrinsic stability of the MoO_x-based contact after module lamination at 150 °C for 20 min. After damp-heat testing (85˚C, 85% humidity, 1000 hours), the power loss of the MoO_x-contacted SHJ mini-module was only 2.8 $\%_{rel}$ and hence the device passes the IEC61215 standard. Controlling thermal history in cell- and module processing, and choosing proper encapsulation material can achieve stably performing TMO based contacts in a module. This work helps to expand the understanding of MoO_x contacts in SHJ solar cells.

Acknowledgments

The authors thank Meric Firat and Arsalan Razzaq for fruitful discussions, and Patrick Carolan and Olivier Richard for the TEM measurements. The authors gratefully acknowledge the financial support of imec's industrial affiliation program for Si-PV. Imec is a partner in EnergyVille (www.energyville.be), a collaboration between the Flemish research partners KU Leuven, VITO, imec, and UHasselt in the field of sustainable energy and intelligent energy systems.

References

[1] D. Adachi, J.L. Hernández, K. Yamamoto, Impact of carrier recombination on fill factor for large area heterojunction crystalline silicon solar cell with 25.1% efficiency, Appl. Phys. Lett. 107 (2015) 233506. doi:10.1063/1.4937224.
[2] Z.C. Holman, A. Descoeudres, L. Barraud, F.Z. Fernandez, J.P. Seif, S. De Wolf, C. Ballif, Current Losses at the Front of Silicon Heterojunction Solar Cells, IEEE J. Photovoltaics. 2 (2012) 7–15. doi:10.1109/JPHOTOV.2011.2174967.
[3] R.A. Street, Hydrogenated amorphous silicon, Cambridge University Press, Cambridge, 1991. doi:10.1017/CBO9780511525247.
[4] A. Paduthol, M.K. Juhl, G. Nogay, P. Löper, T. Trupke, Measuring carrier injection from amorphous silicon into crystalline silicon using photoluminescence, Prog. Photovoltaics Res. Appl. 26 (2018) 968–973. doi:10.1002/pip.3042.
[5] J. Melskens, B.W.H. van de Loo, B. Macco, L.E. Black, S. Smit, W.M.M. Kessels, Passivating Contacts for Crystalline Silicon Solar Cells: From Concepts and Materials to Prospects, IEEE J. Photovoltaics. 8 (2018) 1–16. doi:10.1109/JPHOTOV.2018.2797106.
[6] J. Bullock, Y. Wan, Z. Xu, S. Essig, M. Hettick, H. Wang, W. Ji, M. Boccard, A. Cuevas, C. Ballif, A. Javey, Stable Dopant-Free Asymmetric Heterocontact Silicon Solar Cells with Efficiencies above 20%, ACS Energy Lett. 3 (2018) 508–513. doi:10.1021/acsenergylett.7b01279.
[7] J. Bullock, M. Hettick, J. Geissbühler, A.J. Ong, T. Allen, C.M. Sutter-Fella, T. Chen, H. Ota, E.W. Schaler, S. De Wolf, C. Ballif, A. Cuevas, A. Javey, Efficient silicon solar cells with dopant-free asymmetric heterocontacts, Nat. Energy. 1 (2016) 15031. doi:10.1038/nenergy.2015.31.
[8] J. Cho, J. Melskens, M. Debucquoy, M. Recamán Payo, S. Jambaldinni, T. Bearda, I. Gordon, J. Szlufcik, W.M.M. Kessels, J. Poortmans, Passivating electron-selective contacts for silicon solar cells based on an a-Si:H/TiOx stack and a low work function metal, Prog. Photovoltaics Res. Appl. 26 (2018) 835–845. doi:10.1002/pip.3023.
[9] J. Cho, M. Debucquoy, M.R. Payo, E. Schapmans, I. Gordon, J. Szlufcik, J. Poortmans, Evidence of TiOx reduction at the SiOx/TiOx interface of passivating electron-selective contacts, in: SiliconPV Conf. 2018, 2018: p. 040005. doi:10.1063/1.5049268.
[10] J. Cho, M. Debucquoy, M. Recaman Payo, S. Malik, M. Filipič, H.S. Radhakrishnan, T. Bearda, I. Gordon, J. Szlufcik, J. Poortmans, Contact resistivity reduction on lowly-doped n-type Si using a low work function metal and a thin TiOx interfacial layer for doping-free Si solar cells, in: SiliconPV Conf. 2017, 2017: pp. 842–850. doi:10.1016/j.egypro.2017.09.356.
[11] X. Yang, Q. Bi, H. Ali, K. Davis, W V Schoenfeld, K. Weber, High-Performance TiO2-Based Electron-Selective Contacts for Crystalline Silicon Solar Cells, Adv. Mater. 28 (2016) 5891–5897. doi:10.1002/adma.201600926.
[12] X. Yang, P. Zheng, Q. Bi, K. Weber, Silicon heterojunction solar cells with electron selective TiOx contact, Sol. Energy Mater. Sol. Cells. 150 (2016) 32–38. doi:10.1016/j.solmat.2016.01.020.
[13] D. Sacchetto, Q. Jeangros, G. Christmann, L. Barraud, A. Descoeudres, J. Geissbuhler, M. Despeisse, A. Hessler-Wyser, S. Nicolay, C. Ballif, ITO/MoOx/a-Si:H(i) Hole-Selective Contacts for Silicon Heterojunction Solar Cells: Degradation Mechanisms and Cell Integration, IEEE J. Photovoltaics. 7 (2017) 1584–1590. doi:10.1109/JPHOTOV.2017.2756066.
[14] B. Macco, M.F.J. Vos, N.F.W. Thissen, A.A. Bol, W.M.M. Kessels, Low-temperature atomic layer deposition of MoOx for silicon heterojunction solar cells, Phys. Status Solidi - Rapid Res. Lett. 9 (2015) 393–396. doi:10.1002/pssr.201510117.
[15] T. Zhang, C.-Y. Lee, Y. Wan, S. Lim, B. Hoex, Investigation of the thermal stability of MoOx as hole-selective contacts for Si solar cells, J. Appl. Phys. 124 (2018) 073106. doi:10.1063/1.5041774.
[16] R.A. Vijayan, S. Essig, S. De Wolf, B.G. Ramanathan, P. Loper, C. Ballif, M. Varadharajaperumal, Hole-Collection Mechanism in Passivating Metal-Oxide Contacts on Si Solar Cells: Insights from Numerical Simulations, IEEE J. Photovoltaics. 8 (2018) 473–482. doi:10.1109/JPHOTOV.2018.2796131.

[17] J. Bullock, A. Cuevas, T. Allen, C. Battaglia, Molybdenum oxide MoOx : A versatile hole contact for silicon solar cells, Appl. Phys. Lett. 105 (2014) 232109. doi:10.1063/1.4903467.
[18] C. Battaglia, X. Yin, M. Zheng, I.D. Sharp, T. Chen, S. McDonnell, A. Azcatl, C. Carraro, B. Ma, R. Maboudian, R.M. Wallace, A. Javey, Hole Selective MoOx Contact for Silicon Solar Cells, Nano Lett. 14 (2014) 967–971. doi:10.1021/nl404389u.
[19] L.G. Gerling, S. Mahato, A. Morales-Vilches, G. Masmitja, P. Ortega, C. Voz, R. Alcubilla, J. Puigdollers, Transition metal oxides as hole-selective contacts in silicon heterojunctions solar cells, Sol. Energy Mater. Sol. Cells. 145 (2016) 109–115. doi:10.1016/j.solmat.2015.08.028.
[20] J. Geissbühler, J. Werner, S. Martin De Nicolas, L. Barraud, A. Hessler-Wyser, M. Despeisse, S. Nicolay, A. Tomasi, B. Niesen, S. De Wolf, C. Ballif, 22.5% efficient silicon heterojunction solar cell with molybdenum oxide hole collector, Appl. Phys. Lett. 107 (2015) 081601. doi:10.1063/1.4928747.
[21] L. Neusel, M. Bivour, M. Hermle, Selectivity issues of MoOx based hole contacts, in: SiliconPV Conf. 2017, 2017: pp. 425–434. doi:10.1016/j.egypro.2017.09.268.
[22] S. Essig, J. Dréon, E. Rucavado, M. Mews, T. Koida, M. Boccard, J. Werner, J. Geissbühler, P. Löper, M. Morales-Masis, L. Korte, S. De Wolf, C. Ballif, Toward Annealing-Stable Molybdenum-Oxide-Based Hole-Selective Contacts For Silicon Photovoltaics, Sol. RRL. 2 (2018) 1700227. doi:10.1002/solr.201700227.
[23] M.A. Sen, P. Spinelli, B. Kikkert, E. Hoek, B. Macco, A. Weeber, P. Bronsveld, Electron beam evaporated molybdenum oxide as hole-selective contact in 6-inch c-Si heterojunction solar cells, in: AIP Conf. Proc., 2018: p. 040001. doi:10.1063/1.5049264.
[24] K. Mallem, Y.J. Kim, S.Q. Hussain, S. Dutta, A.H.T. Le, M. Ju, J. Park, Y.H. Cho, Y. Kim, E.-C. Cho, J. Yi, Molybdenum oxide: A superior hole extraction layer for replacing p-type hydrogenated amorphous silicon with high efficiency heterojunction Si solar cells, Mater. Res. Bull. 110 (2019) 90–96. doi:10.1016/j.materresbull.2018.10.018.
[25] M.T. Greiner, L. Chai, M.G. Helander, W.M. Tang, Z.H. Lu, Transition metal oxide work functions: The influence of cation oxidation state and oxygen vacancies, Adv. Funct. Mater. 22 (2012) 4557–4568. doi:10.1002/adfm.201200615.
[26] G. Gregory, M. Wilson, H. Ali, K.O. Davis, Thermally Stable Molybdenum Oxide Hole-Selective Contacts Deposited using Spatial Atomic Layer Deposition, 2018 IEEE 7th World Conf. Photovolt. Energy Convers. (A Jt. Conf. 45th IEEE PVSC, 28th PVSEC 34th EU PVSEC). (2018) 2006–2009. doi:10.1109/PVSC.2018.8547343.
[27] N. Miyata, T. Suzuki, R. Ohyama, Physical properties of evaporated molybdenum oxide films, Thin Solid Films. 281–282 (1996) 218–222. doi:10.1016/0040-6090(96)08617-8.
[28] M. Gao, D. Chen, B. Han, W. Song, M. Zhou, X. Song, F. Xu, L. Zhao, Y. Li, Z. Ma, Bifunctional Hybrid a-SiOx (Mo) Layer for Hole-Selective and Interface Passivation of Highly Efficient MoOx /a-SiOx (Mo)/n-Si Heterojunction Photovoltaic Device, ACS Appl. Mater. Interfaces. 10 (2018) 27454–27464. doi:10.1021/acsami.8b07001.
[29] M. Higuchi, S. Uekusa, R. Nakano, K. Yokogawa, Postdeposition Annealing Influence on Sputtered Indium Tin Oxide Film Characteristics, Jpn. J. Appl. Phys. 33 (1994) 302–306. doi:10.1143/JJAP.33.302.
[30] B. Demaurex, S. De Wolf, A. Descoeudres, Z. Charles Holman, C. Ballif, Damage at hydrogenated amorphous/crystalline silicon interfaces by indium tin oxide overlayer sputtering, Appl. Phys. Lett. 101 (2012) 1–5. doi:10.1063/1.4764529.
[31] J. Werner, J. Geissbühler, A. Dabirian, S. Nicolay, M. Morales-Masis, S. De Wolf, B. Niesen, C. Ballif, Parasitic Absorption Reduction in Metal Oxide-Based Transparent Electrodes: Application in Perovskite Solar Cells, ACS Appl. Mater. Interfaces. 8 (2016) 17260–17267. doi:10.1021/acsami.6b04425.
[32] A. Borgschulte, O. Sambalova, R. Delmelle, S. Jenatsch, R. Hany, F. Nüesch, Hydrogen reduction of molybdenum oxide at room temperature, Sci. Rep. 7 (2017) 40761. doi:10.1038/srep40761.
[33] B. Paviet-Salomon, A. Tomasi, A. Descoeudres, L. Barraud, S. Nicolay, M. Despeisse, S.D. Wolf, C. Ballif, Back-Contacted Silicon Heterojunction Solar Cells: Optical-Loss Analysis and

Mitigation, IEEE J. Photovoltaics. 5 (2015) 1293–1303. doi:10.1109/JPHOTOV.2015.2438641.
[34] S. Il Park, S. Jae Baik, J.-S. Im, L. Fang, J.-W. Jeon, K. Su Lim, Towards a high efficiency amorphous silicon solar cell using molybdenum oxide as a window layer instead of conventional p-type amorphous silicon carbide, Appl. Phys. Lett. 99 (2011) 063504. doi:10.1063/1.3624591.
[35] K.H. Wong, K. Ananthanarayanan, J. Luther, P. Balaya, Origin of hole selectivity and the role of defects in low-temperature solution-processed molybdenum oxide interfacial layer for organic solar cells, J. Phys. Chem. C. 116 (2012) 16346–16351. doi:10.1021/jp303679y.
[36] R.A.. H. Khanna T.; Stangl B.; Basu, P. K.; Aberle, A. G., A.; Mueller, A. Khanna, T. Mueller, R.A. Stangl, B. Hoex, P.K. Basu, A.G. Aberle, A Fill Factor Loss Analysis Method for Silicon Wafer Solar Cells, IEEE J. Photovoltaics,. 3 (2013) 1170–1177. doi:10.1109/JPHOTOV.2013.2270348.
[37] S. Bowden, A. Rohatgi, Rapid and accurate determination of series resistance and fill factor losses in industrial silicon solar cells, in: 17th Eur. Photovolt. Sol. Energy Conf. Exhib., Munich, Germany, 2001.
[38] L.G. Gerling, C. Voz, R. Alcubilla, J. Puigdollers, Origin of passivation in hole-selective transition metal oxides for crystalline silicon heterojunction solar cells, J. Mater. Res. 32 (2017) 260–268. doi:10.1557/jmr.2016.453.
[39] H. Ali, J. Bullock, G. Gregory, X. Yang, M. Schneider, K. Weber, K.O. Davis, M. Science, C. Florida, Transmission Electron Microscopy Studies of Transition Metal Oxides Employed as Carrier Selective Contacts in Silicon Solar Cells, in: World Conf. Photovolt. Energy Convers., Waikoloa, Hi, USA, 2018: pp. 3–5.
[40] H. Ali, S. Koul, G. Gregory, J. Bullock, A. Javey, A. Kushima, K.O. Davis, In Situ Transmission Electron Microscopy Study of Molybdenum Oxide Contacts for Silicon Solar Cells, Phys. Status Solidi Appl. Mater. Sci. 1800998 (2019) 1–4. doi:10.1002/pssa.201800998.
[41] D. Das, S.M. Iftiquar, A.K. Barua, Wide optical-gap a-SiO:H films prepared by rf glow discharge, J. Non. Cryst. Solids. 210 (1997) 148–154. doi:10.1016/S0022-3093(96)00597-2.
[42] Y. Zhang, C. Yu, M. Yang, Y. He, L. Zhang, J. Zhang, X. Xu, Y. Zhang, X. Song, H. Yan, Optimization of the window layer in large area silicon heterojunction solar cells, RSC Adv. 7 (2017) 9258–9263. doi:10.1039/C6RA26342A.
[43] I. Irfan, Y. Gao, Effects of exposure and air annealing on MoOx thin films, J. Photonics Energy. 2 (2012) 021213. doi:10.1117/1.JPE.2.021213.
[44] M. Bivour, F. Zähringer, P. Ndione, M. Hermle, Sputter-deposited WOx and MoOx for hole selective contacts, in: SiliconPV Conf. 2017, 2017: pp. 400–405. doi:10.1016/j.egypro.2017.09.259.
[45] Z. Liang, M. Su, Y. Zhou, L. Gong, C. Zhao, K. Chen, F. Xie, W. Zhang, J. Chen, P. Liu, W. Xie, Interaction at the silicon/transition metal oxide heterojunction interface and its effect on the photovoltaic performance, Phys. Chem. Chem. Phys. 17 (2015) 27409–27413. doi:10.1039/C5CP05309A.
[46] S. Essig, J. Dréon, J. Werner, P. Löper, S. De Wolf, M. Boccard, C. Ballif, MoOx and WOx based hole-selective contacts for wafer-based Si solar cells, in: 44th IEEE Photovolt. Spec. Conf., 2017: pp. 2–5.